Reduced order modelling for the nonlinear geometric response of some curved structures

Y.-W. Chang, X.Q. Wang, Evangéline Capiez-Lernout, M. P. Mignolet, Christian Soize

REDUCED ORDER MODELING FOR THE NONLINEAR GEOMETRIC RESPONSE OF SOME CURVED STRUCTURES

Y.-W. Chang [1], X.Q. Wang [1], E. Capiez-Lernout [2], M.- P. Mignolet [1], C. Soize [2]

[1] SEMTE, Faculties of Mechanical and Aerospace Engineering
Arizona State University, Tempe, AZ 85287-6106, USA
ychang39@asu.edu, xiaoquan.wang.1@asu.edu, marc.mignolet@asu.edu

[2] Laboratoire de Modélisation et Simulation Multi Echelle,
Université Paris-Est, 5 bd Descartes, 77455 Marne-la-Vallée Cedex 02, France
evangeline.capiezlernout@univ-paris-est.fr, christian.soize@univ-paris-est.fr

Keywords: reduced order models, nonlinear geometric, panels, wings, curved structures.

Abstract: The focus of this paper is on the assessment of nonlinear reduced order models (ROM) for the accurate prediction of the geometrically nonlinear response of some curved structures. Earlier difficulties in obtaining accurate reduced order models are clarified and a revised identification procedure of the ROM parameters is proposed. The validation of the methodology to a curved beam and a cylindrical shell, in full 3-D displacements, are presented. The excellent matching between full finite element and ROM predicted responses demonstrate the value of the approach.

1 INTRODUCTION

Modal models have long been recognized as the computationally efficient analysis method of complex linear structural dynamic systems, yielding a large reduction in computational cost but also allowing a convenient coupling with other physics code, e.g. with aerodynamics/CFD codes for aeroelastic analyses. Further, these modal models are easily derived from a finite element model of the structure considered and thus can be obtained even for complex geometries and boundary conditions. However, a growing number of applications require the consideration of geometric nonlinearity owing to the large structural displacements. For example, panels of supersonic/hypersonic vehicles have often in the past been treated in this manner because of the large acoustic loading they are subjected to as well as possible thermal effects. Novel, very flexible air vehicles have provided another, more recent class of situations in which geometric nonlinearity must be included.

For such problems, it would be very desirable to have the equivalent of the modal methods exhibiting: (i) high computational efficiency, (ii) an ease of coupling to other physics codes, and (iii) generality with respect to the structure considered and its boundary conditions. To this end, nonlinear reduced order modeling techniques have been proposed and validated in the last decade [1-13]. Although several variants exist, their construction share the same aspects. First, they involve a *parametric* form of the model, i.e. one in which the nonlinearity is only on the "stiffness" and includes linear, quadratic, and cubic terms of the displacement field generalized coordinates (see section below). Second, they rely on an identification strategy of the parameters of the model, i.e. the linear, quadratic, and cubic stiffness coefficients, from a finite element model of the structure for a particular set of "modes" or basis functions. Differences between the existing methods center in particular on the way the linear and nonlinear stiffness coefficients are estimated from a finite element

model and on the extent and specificity of the basis functions, i.e. modeling of only the displacements transverse to the structure or all of them.

As may be expected, the first validations of these reduced order models focused on flat structures, beams and plates, and an excellent match between responses predicted by the reduced order models and their full finite element counterparts have been demonstrated. Curved structures, curved beam most notably, have also been investigated in the last few years and a very good match of reduced order model and full finite element results was obtained. Yet, the construction of the reduced order model was not as straightforward in this case as it had been in flat structures, instabilities of the model were sometime obtained.

The issue of constructing stable and accurate nonlinear reduced order models for curved structures is revisited here and an extension of the displacement-based (STEP) identification procedure [14,8] is first proposed. Then, its applications to a curved beam model and to a cylindrical shell undergoing multi directional loading are demonstrated, and shown to lead to an excellent matching between reduced order model and full finite element predictions.

2 PARAMETRIC FORM OF NONLINEAR REDUCED ORDER MODELS

The reduced order models considered here are representations of the response of elastic geometrically nonlinear structures in the form

$$u_i(\underline{X},t) = \sum_{n=1}^{M} q_n(t)\, \psi_i^{(n)}(\underline{X}) \ , \ i = 1, 2, 3, \tag{1}$$

where $u_i(\underline{X},t)$ denotes the displacement components at a point $\underline{X}$ of the structure and at time t. Further, $\psi_i^{(n)}(\underline{X})$ are specified, constant basis functions and $q_n(t)$ are the time dependent generalized coordinates.

A general derivation of linear modal models is classically carried out from linear (infinitesimal) elasticity and it is thus desired here to proceed similarly but with finite deformation elasticity to include the full nonlinear geometric effects. Then, the first issue to be addressed is in what configuration, deformed or undeformed, the governing equations ought to be written. In this regard, note that the basis functions $\psi_i^{(n)}(\underline{X})$ are expected to (a) be independent of time and (b) satisfy the boundary conditions (at least the geometric or Dirichlet ones). These two conditions are not compatible if the basis functions are expressed in the deformed configuration as the locations at which the boundaries are will vary with the level of deformations or implicitly with time. However, these conditions are compatible if one proceeds in the undeformed configuration and thus $\underline{X}$ in Eq. (1), will denote the coordinates of a point in the undeformed configuration.

Accordingly, the equations of motion of an infinitesimal element can be expressed as (e.g. see [15,16], summation over repeated indices assumed)

$$\frac{\partial}{\partial X_k}\left(F_{ij}\, S_{jk}\right) + \rho_0\, b_i^0 = \rho_0\, \ddot{u}_i \ \text{ for } \ \underline{X} \in \Omega_0 \,, \tag{2}$$

where S denotes the second Piola-Kirchhoff stress tensor, ρ_0 is the density in the reference configuration, and $\underline{b}^0$ is the vector of body forces, all of which are assumed to depend on the coordinates X_i. Further, in Eq. (2), the deformation gradient tensor F is defined by its components F_{ij} as

$$F_{ij} = \frac{\partial x_i}{\partial X_j} = \delta_{ij} + \frac{\partial u_i}{\partial X_j}, \tag{3}$$

where δ_{ij} denotes the Kronecker symbol and the displacement vector is $\underline{u} = \underline{x} - \underline{X}$, $\underline{x}$ being the position vector in the deformed configuration. Finally, Ω_0 denotes the domain occupied by the structure in the undeformed configuration. It has a boundary $\partial\Omega_0$ composed of two parts: $\partial\Omega_0^t$ on which the tractions $\underline{t}^0$ are given and $\partial\Omega_0^u$ on which the displacements are specified (assumed zero here). Thus, the boundary conditions associated to Eq. (2) are

$$F_{ij}\, S_{jk}\, n_k^0 = t_i^0 \quad \text{for } \underline{X} \in \partial\Omega_0^t, \tag{4}$$

$$\underline{u} = \underline{0} \quad \text{for } \underline{X} \in \partial\Omega_0^u. \tag{5}$$

Note in Eqs (2) and (4) that the vectors $\underline{b}^0$ and $\underline{t}^0$ correspond to the transport ("pull back") of the body forces and tractions applied on the deformed configuration, i.e. $\underline{b}$ and $\underline{t}$, back to the reference configuration (see [15,16]).

To complete the formulation of the elastodynamic problem, it remains to specify the constitutive behavior of the material. In this regard, it will be assumed here that the second Piola-Kirchhoff stress tensors S is linearly related to the Green strain tensor E defined as

$$E_{ij} = \frac{1}{2}\left(F_{ki}\, F_{kj} - \delta_{ij}\right). \tag{6}$$

That is,

$$S_{ij} = C_{ijkl}\, E_{kl}\ , \tag{7}$$

where C_{ijkl} denotes the fourth order elasticity tensor.

Introducing the assumed displacement field of Eq. (1) in Eqs (2)-(7) and proceeding with a Galerkin approach leads, after some manipulations, to the desired governing equations, i.e.

$$M_{ij}\ddot{q}_j + D_{ij}\dot{q}_j + K_{ij}^{(1)}\, q_j + K_{ijl}^{(2)} q_j q_l + K_{ijlp}^{(3)} q_j q_l q_p = F_i \tag{8}$$

in which M_{ij} are mass components, $K_{ij}^{(1)}$, $K_{ijl}^{(2)}$, and $K_{ijlp}^{(3)}$ are the linear, quadratic, and cubic stiffness coefficients, and F_i are the modal forces. Note that the damping term $D_{ij}\,\dot{q}_j$ has been added in Eq. (8) to collectively represent various dissipation mechanisms. Further,

the symmetrical role of j and l in the quadratic terms and j, l, and p in the cubic ones indicates that the summations over those indices can be restricted to $p \geq l \geq j$.

Once the generalized coordinates $q_j(t)$ have been determined from Eq. (8), the stress field can also be evaluated from Eqs. (3), (6), and (7). Specifically, it is found that every component of the second Piola-Kirchhoff stress tensor can be expressed as

$$S_{ij} = \overline{S}_{ij} + \sum_m \hat{S}_{ij}^{(m)} q_m + \sum_{m,n} \widetilde{S}_{ij}^{(m,n)} q_m q_n \,, \tag{9}$$

where the coefficients $\overline{S}_{ij}$, $\hat{S}_{ij}^{(m)}$, and $\widetilde{S}_{ij}^{(m,n)}$ depend only on the point $\underline{X}$ considered.

3 IDENTIFICATION OF THE REDUCED ORDER MODEL PARAMETERS

One of the key component of the present as well as related nonlinear reduced order modeling approaches (see introduction) is the identification of the parameters of Eqs (8) and (9) from a finite element model of the structure considered in a standard (e.g. Nastran, Abaqus, Ansys) software. The reliance of such commercial codes gives access to a broad database of elements, boundary conditions, numerical algorithms, etc. but is a challenge from the standpoint of the determination of the parameters of Eqs (8) and (9) as one has only limited access to the detailed element information and matrices.

In a finite element format, the displacement field of components $u_i(\underline{X},t)$ is replaced by its discretized counterpart, the vector $\underline{u}(t)$, represented as

$$\underline{u}(t) = \sum_{n=1}^{M} q_n(t)\, \underline{\Psi}^{(n)} \tag{10}$$

where $\underline{\Psi}^{(n)}$ are the discretized basis functions. The estimation of the mass components M_{ij} and modal forces F_i is achieved as in linear modal models, i.e.

$$M_{ij} = \underline{\Psi}^{(i)T}\, M_{FE}\, \underline{\Psi}^{(j)} \qquad\qquad F_i = \underline{\Psi}^{(i)T}\, \underline{F}(t) \tag{11a), (11b)}$$

where M_{FE} is the finite element mass matrix and $\underline{F}(t)$ is the excitation vector on the structure.

Next is the determination of the stiffness coefficients $K_{ij}^{(1)}$, $K_{ijl}^{(2)}$, and $K_{ijlp}^{(3)}$. In this regard, note first that the linear coefficients $K_{ij}^{(1)}$ could be determined as in linear modal models, i.e.

$$K_{ij}^{(1)} = \underline{\Psi}^{(i)T}\, K_{FE}^{(1)}\, \underline{\Psi}^{(j)} \tag{12}$$

where $K_{FE}^{(1)}$ is the finite element linear stiffness matrix. Another approach must be adopted however for $K_{ijl}^{(2)}$ and $K_{ijlp}^{(3)}$ as nonlinear stiffness matrices are typically not available. Two approaches have been proposed to identify these parameters (and potentially the linear ones as well) from a series of static finite element solutions. The first one relies on prescribing a series of load cases and projecting the induced responses on the basis functions $\underline{\psi}^{(n)}$ to obtain the corresponding generalized coordinates values $q_j^{(p)}$, p being the index of the load cases. Then, introducing these values into Eq. (8) for each load case yields

$$K_{ij}^{(1)}\, q_j^{(p)} + K_{ijl}^{(2)} q_j^{(p)} q_l^{(p)} + K_{ijlr}^{(3)}\, q_j^{(p)} q_l^{(p)} q_r^{(p)} = F_i^{(p)},\ i = 1, ..., M\,. \qquad (13)$$

Proceeding similarly for P load cases yields a set of linear algebraic equations for the coefficients $K_{ijl}^{(2)}$ and $K_{ijlp}^{(3)}$, and possibly the linear stiffness coefficients $K_{ij}^{(1)}$ as well, which can be solved in a least squares format to complete the identification of the stiffness parameters.

An alternate strategy has also been proposed (e.g. see [14]) in which the *displacements* are prescribed and the required force distributions are obtained from the finite element code. The corresponding modal forces are then evaluated from Eq. (11b) and a set of equations of the form of Eq. (13) is again obtained. Appropriately selecting the displacement fields to be imposed can lead to a particularly convenient identification of the stiffness coefficients. Specifically, the imposition of displacements proportional to the basis function $\underline{\psi}^{(n)}$ only, i.e.

$$\underline{u} = q_n\ \underline{\psi}^{(n)} \qquad \underline{\hat{u}} = \hat{q}_n\ \underline{\psi}^{(n)} \qquad \underline{\tilde{u}} = \tilde{q}_n\ \underline{\psi}^{(n)} \qquad (14)$$

leads to the 3 sets of equations

$$\begin{aligned}
&K_{in}^{(1)}\, q_n + K_{inn}^{(2)} q_n^2 + K_{innn}^{(3)}\, q_n^3 = F_i \quad \text{(no sum on } n\text{)}\\
&K_{in}^{(1)}\, \hat{q}_n + K_{inn}^{(2)} \hat{q}_n^2 + K_{innn}^{(3)}\, \hat{q}_n^3 = \hat{F}_i \quad \text{(no sum on } n\text{)}\\
&K_{in}^{(1)}\, \tilde{q}_n + K_{inn}^{(2)} \tilde{q}_n^2 + K_{innn}^{(3)}\, \tilde{q}_n^3 = \tilde{F}_i \quad \text{(no sum on } n\text{)}
\end{aligned} \qquad (15)$$

in which no sum over the index n is to be understood and for $i = 1, ..., M$. In fact, these 3 sets of equations permit the direct evaluation of the coefficients $K_{in}^{(1)}$, $K_{inn}^{(2)}$, and $K_{innn}^{(3)}$ for all i. Repeating this effort for $n = 1, ..., M$ thus yields a first set of stiffness coefficients.

Proceeding similarly but with combinations of two basis functions, i.e.

$$\underline{u} = q_n\ \underline{\psi}^{(n)} + q_m\ \underline{\psi}^{(m)} \quad m \geq n \qquad (16)$$

and relying on the availability of the coefficients $K_{in}^{(1)}$, $K_{inn}^{(2)}, K_{innn}^{(3)}$ and $K_{im}^{(1)}$, $K_{imm}^{(2)}$, $K_{immm}^{(3)}$ determined above, leads to equations involving the three coefficients $K_{inm}^{(2)}$, $K_{innm}^{(3)}$, and $K_{inmm}^{(3)}$. Thus, imposing three sets of displacements of the form of Eq. (16) provides the equations needed to also identify $K_{inm}^{(2)}$, $K_{innm}^{(3)}$, and $K_{inmm}^{(3)}$.

Finally, imposing displacement fields linear combination of three modes, i.e.

$$\underline{u} = q_n \ \underline{\Psi}^{(n)} + q_m \ \underline{\Psi}^{(m)} + q_r \ \underline{\Psi}^{(r)} \qquad r \geq m \geq n \tag{17}$$

permits the identification of the last coefficients, i.e. $K_{inmr}^{(3)}$.

The above approach, referred to as the STEP (STiffness Evaluation Procedure), has often been used and has generally led to the reliable identification of the reduced order model parameters, especially in connection with flat structures, with values of the generalized coordinates q_s of the order of, or small than, the thickness. However, in some curved structures, e.g. the curved beam of [11], several of the models identified by the STEP process were found to be unstable, i.e. a finite static solution could not be obtained with a time marching algorithm, when the applied load magnitude exceeded a certain threshold. This problem occurred most notably for loads inducing a snap-through of the curved beam.

In studying this problem, it was observed that the magnitude of some of the terms $K_{ij}^{(1)} q_j$, $K_{ijl}^{(2)} q_j q_l$, and/or $K_{ijlr}^{(3)} q_j q_l q_r$ computed at a large amplitude (of the order of 10 thicknesses say) snap-through solution were much larger (2 orders of magnitude was routinely observed) than the driving $F_i^{(p)}$. Accordingly, the balance of the terms on the left-hand-side of Eq. (8) must be accomplished quite accurately or, equivalently, a very good accuracy is required on the stiffness coefficients, to have a good match of the full finite element solution in such cases. A sensitivity analysis of the stiffness coefficients identified by the above approach in the curved beam case (see description below) suggested that the accuracy requirements were right at the limit of what could be expected and thus another identification procedure was sought.

The perceived weakness of the procedure based on Eqs (14)-(17) is that the identification is conducted near the undeformed configuration for which the linear terms are much larger than the quadratic ones, themselves much larger than the cubic terms. That is, in conditions in which the critical balance of the terms on the left-hand-side does not take place. In this light, it was proposed to shift the baseline point around which the identification is achieved from the undeformed state to one in or near the expected difficult conditions, e.g. in a snap-through configuration for the curved beam. This baseline solution admits the representation

$$\underline{u}_0 = \sum_{n=1}^{M} q_{n,0} \ \underline{\Psi}^{(n)} \ . \tag{18}$$

Then, the test displacement fields imposed for identification are

$$\underline{u} = \underline{u}_0 + q_n \ \underline{\Psi}^{(n)} \tag{19}$$

$$\underline{u} = \underline{u}_0 + q_n \ \underline{\Psi}^{(n)} + q_m \ \underline{\Psi}^{(m)} \quad m \geq n \tag{20}$$

$$\underline{u} = \underline{u}_0 + q_n \ \underline{\Psi}^{(n)} + q_m \ \underline{\Psi}^{(m)} + q_r \ \underline{\Psi}^{(r)} \quad r \geq m \geq n \, . \tag{21}$$

More specifically, for each value of n = 1, ..., M, three cases of the form of Eq. (19) were considered with q_n = +q, -q, and q/2 as before with q typically smaller than the thickness. The four cases corresponding to positive and negative values of q_n and q_m in Eq. (20) were also included for each n and $m \geq n$. Finally, all eight cases associated with positive and negative values of q_n, q_m, and q_r for $r \geq m \geq n$ and all n were used.

The displacement fields of Eqs (19)-(21) include generalized coordinates along all basis functions and thus no simplification of Eq. (13) takes place as in Eq. (15). Accordingly, the stiffness coefficients were obtained by a least squares solution of Eq. (13) with the complete set of displacement fields imposed by Eq. (19)-(21). Note that the linear, quadratic, and cubic stiffness coefficients are often of very different magnitudes and thus an appropriate scaling of the terms is recommended to keep low the condition number of the least squares matrix. It was also found beneficial to include the equations corresponding to two different baseline displacement fields $\underline{u}_0$.

4 BASIS SELECTION

The two previous sections have focused on the derivation of the parametric form of the reduced order model governing equations, Eqs (8) and (13), and on the estimation of the parameters from a set of well chosen finite element solutions. The last key aspect of the construction of reduced order models is the selection of the basis functions $\underline{\Psi}^{(n)}$. In this regard, the expected features of the reduced order model are that (i) it leads to an accurate representation of the full finite element results and (ii) it includes a "reasonably" small number of basis functions. To satisfy these requirements, these functions should closely capture the expected physics of the structural response and recent research efforts have focused on this issue [8,12,13]. In particular, it was proposed in [8] to complement the basis functions that would be used in a linear analysis by functions, referred to as the dual modes, that would capture the nonlinear interactions in the structure.

While the construction of the dual modes is applicable to any structural modeling, it is most easily described in the context of an isotropic flat structure, e.g. beam or plate, subjected to a transverse loading. Selecting an appropriate basis for the transverse displacements follows the same steps as in a linear analysis in which no further modeling is necessary. When the response level is large enough for nonlinear geometric effects to be significant, small in-plane displacements appear in the full solution which are associated with the "membrane stretching" effect. While small, these in-plane motions induce a significant softening of the stiffening nonlinearity associated with pure transverse motions.

One approach to construct a full basis, i.e. modeling both transverse and in-plane displacements, appropriate for the modeling of the nonlinear response is to focus specifically on capturing the membrane stretching effects. The key idea in this approach is thus to

subject the structure to a series of "representative" static loadings, determine the corresponding *nonlinear* displacement fields, and extract from them additional basis functions, referred to as the "dual modes" that will be appended to the linear basis, i.e. the modes that would be used in the linear case.

In this regard, note that the membrane stretching effect is induced by the nonlinear interaction of the transverse and in-plane displacements, not by an external loading. Thus, the dual modes can be viewed as associated (the adjective "companion" would have been a better description than "dual") with the transverse displacements described by the linear basis. The representative static loadings should then be selected to excite primarily the linear basis functions and, in fact, in the absence of geometric nonlinearity (i.e. for a linear analysis) should only excite these "modes". This situation occurs when the applied load vectors on the structural finite element model are of the form

$$\underline{F}^{(m)} = \sum_i \alpha_i^{(m)} \, K_{FE}^{(1)} \, \underline{\psi}^{(i)} \tag{22}$$

where $\alpha_i^{(m)}$ are coefficients to be chosen with *m* denoting the load case number. A detailed discussion of the linear combinations to be used is presented in [8] but, in all validations carried out, it has been sufficient to consider the cases

$$\underline{F}_i^{(m)} = \alpha_i^{(m)} \, K_{FE}^{(1)} \, \underline{\psi}^{(i)} \qquad i = \text{dominant mode} \tag{23}$$

and

$$\underline{F}_{ij}^{(m)} = \frac{\alpha_i^{(m)}}{2} \left[K_{FE}^{(1)} \, \underline{\psi}^{(i)} \; K_{FE}^{(1)} \, \underline{\psi}^{(j)} \right] \qquad i = \text{dominant mode}, \; j \neq i \tag{24}$$

where a "dominant" mode is loosely defined as one providing a large component of the response. The ensemble of loading cases considered is formed by selecting several values of $\alpha_i^{(m)}$ for each dominant mode in Eq. (23) and also for each mode $j \neq i$ in Eq. (24). Note further that both positive and negative values of $\alpha_i^{(m)}$ are suggested and that their magnitudes should be such that the corresponding displacement fields $\underline{u}_i^{(m)}$ and $\underline{u}_{ij}^{(m)}$ range from near linear cases to some exhibiting a strong nonlinearity.

The next step of the basis construction is the extraction of the nonlinear effects in the obtained displacement fields which is achieved by removing from the displacements fields their projections on the linear basis, i.e. by forming the vectors

$$\underline{v}_i^{(m)} = u_i^{(m)} - \sum_s \left\lfloor \underline{\psi}_s^T \, M \, u_i^{(m)} \right\rfloor \underline{\psi}_s \qquad \text{and} \qquad \underline{v}_{ij}^{(m)} = u_{ij}^{(m)} - \sum_s \left\lfloor \underline{\psi}_s^T \, M \, u_{ij}^{(m)} \right\rfloor \underline{\psi}_s \tag{25}$$

assuming that the finite element mass matrix serves for the orthonormalization of the basis functions $\underline{\psi}^{(n)}$ (including the linear basis functions and any dual mode already selected).

A proper orthogonal decomposition of each set of "nonlinear responses" $\underline{v}_i^{(m)}$ and $\underline{v}_{ij}^{(m)}$ is then sequentially carried out to extract the dominant features of these responses which are then selected as dual modes. The POD eigenvectors $\underline{\phi}_r$ selected as dual modes should not only be associated with a large eigenvalue but should also induce a large strain energy, as measured by $\underline{\phi}_r^T K_{FE}^{(1)} \underline{\phi}_r$, since the membrane stretching that the dual modes are expected to model is a stiff deformation mode.

To exemplify the above process, a flat aluminum beam (see [17] for details), cantilevered on both ends was considered and the duals corresponding to the first four symmetric transverse modes are shown in Fig. 1. Note that these duals are all antisymmetric as expected from the symmetry of the transverse motions assumed. To obtain a better sense of the appropriateness of these functions, a POD analysis of an ensemble of nonlinear responses was carried out and also shown on Fig 1 are the mass normalized POD eigenvectors found for the in-plane displacements. In fact, two such analyses were conducted, one using a series of static responses and the other using snapshots obtained during a dynamic run. It is seen from these results that the dual modes proposed in [8] are in fact very close to the POD eigenvectors obtained from the dynamic snapshots. The difference between POD eigenvectors obtained in static and dynamic conditions can be attributed to the difference in conditions used for their determination.

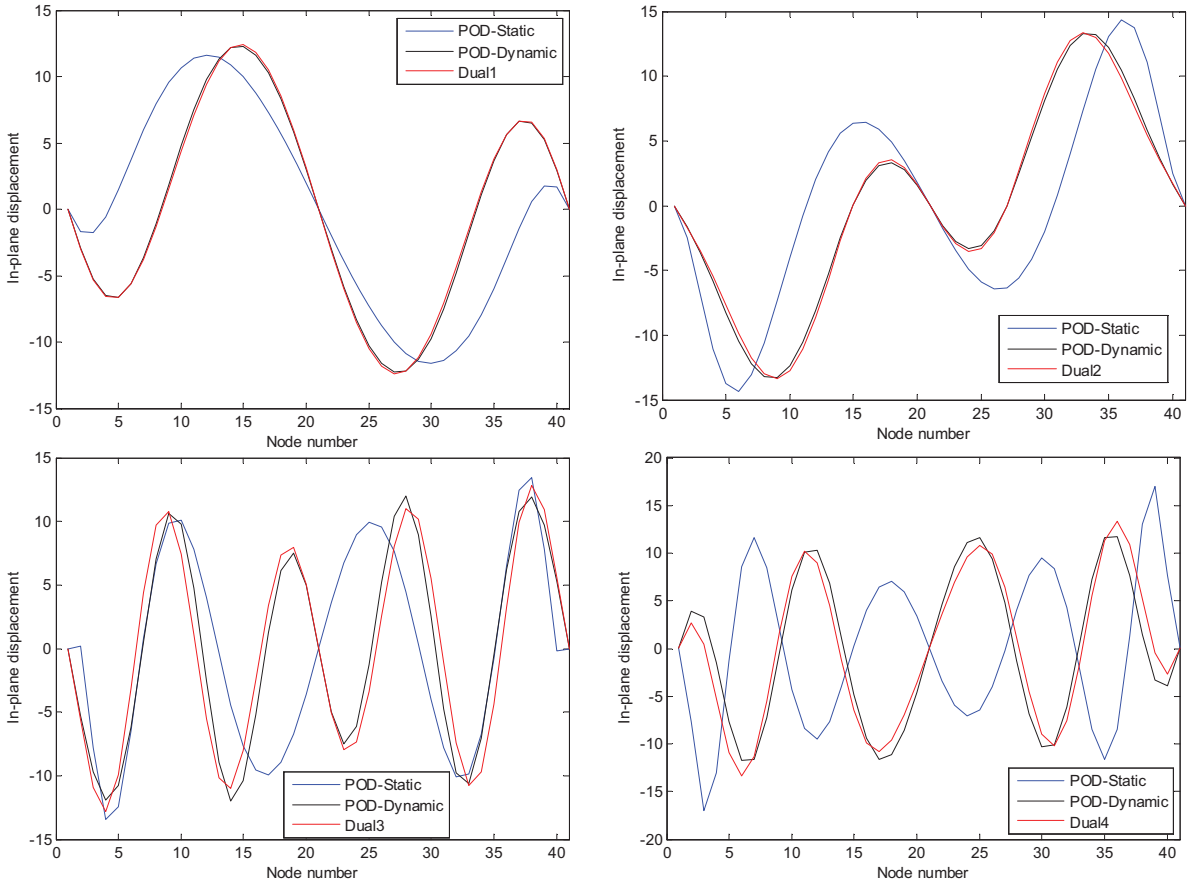

Figure 1. Comparison of dual modes and POD eigenvectors of static and dynamic responses, clamped-clamped flat beam.

5 CURVED BEAM VALIDATION CASE

The first validation case for the identification strategy based on Eqs (19)-(21) is the clamped-clamped curved beam of [4,5,11], see Fig. 2. The beam has an elastic modulus of 10.6×10^6 psi, shear modulus of 4.0×10^6 psi, and density of 2.588×10^{-4} lbf-sec^2/in^4. A Nastran finite element model with 144 CBEAM elements was developed to first construct the reduced order model and then assess its predictive capabilities. The reduced order model development aimed at the dynamic response to a pressure uniform in space but varying in time. The present discussion focuses solely on the static response to such a loading, i.e. $F(t) = P$ constant, and shown in Fig. 3 is the vertical displacement induced at the middle of the beam as a function of P. Note that the beam exhibits a snap-through at $P = 1.89$ lb/in and that the magnitude of the snap-through deformation is quite large, of the order of 10 thicknesses. If the beam is unloaded from this point, it will go back to the neighborhood of the undeformed position, i.e. on the left branch, at a small load of approximately 0.45 lb/in.

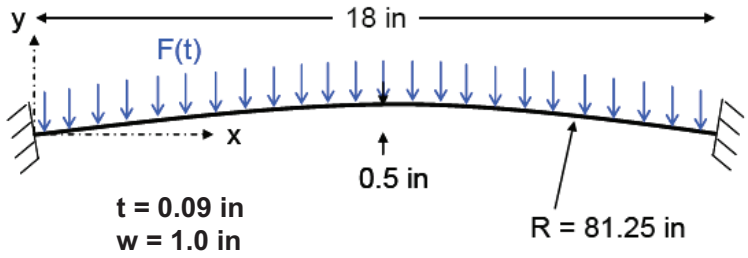

Figure 2. Curved beam geometry.

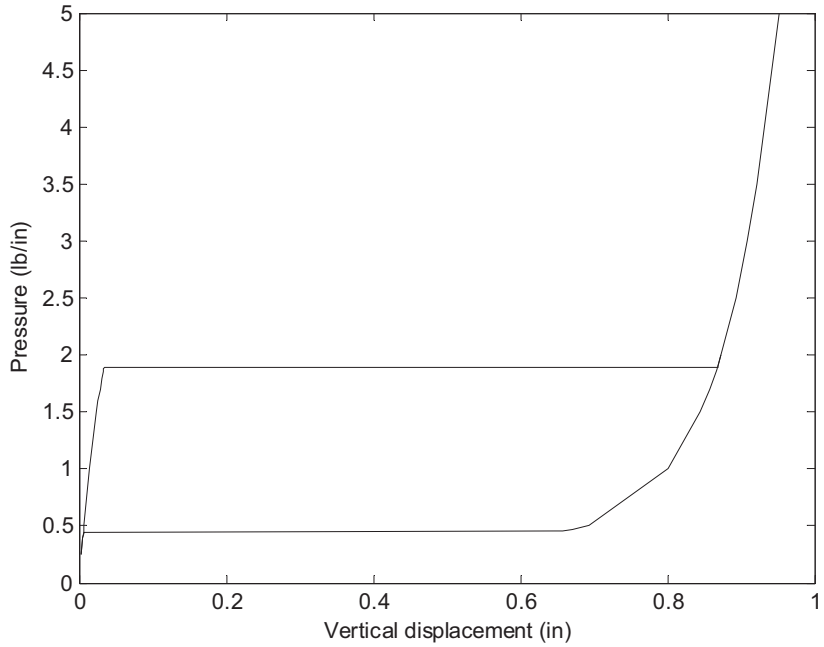

Figure 3. Relation between applied static pressure and vertical displacement of the beam middle, curved beam.

In selecting the basis for the reduced order model, it was recognized that the vertical/normal displacements of the beam to the applied loads are of constant signs, similar in shape to those that would be induced on a flat beam. However, the modes of the curved beam, even the first one, exhibit nodes and thus have variable signs along the beam. This observation suggested in [11] not to use the linear modes of the curved beam, but rather those of the

corresponding straight beam, as the linear basis (see previous section for discussion). These modes were assumed to define the displacement in the locally normal direction to the beam. As in [11], the first 6 such symmetric modes were retained here. The antisymmetric modes do not contribute to the static response and thus are not included here. They are however important for the occurrence of snap-throughs dynamically and are thus considered in dynamic computations (see [17]).

The next step of the reduced order model construction focused on the modeling of the locally tangent displacements which was achieved using the dual modes of section 5 with the first basis function (first mode of the flat beam) dominant. Since the first 6 basis functions included only normal components, the 6 dual modes were made purely tangential by stripping their normal components. This process led for the present static computations to a 12 mode model similar to the one considered in [11], see [17] for additional models and results.

The construction of the reduced order model according to the STEP procedure of Eqs (14)-(17) led to the same difficulties as those encountered in [11] and described in section 3, i.e. difficulty in obtaining a static solution by a time marching integration of the reduced order equations of Eq. (8). Even when a solution could be found, it led to a poor matching of the finite element results. This issue was resolved in [11] by a detailed study of coefficients and a zeroing out of those that drove the instability; a model matching well the full finite element results was then obtained.

The present effort relied instead on the revised identification procedure, i.e. Eqs (18)-(22). Specifically, two baseline solutions were considered that correspond to the projection of the full finite element results at P = 1.7lb/in on the left branch, i.e. below the snap-through limit, and at P = 2lb/in, i.e. above the snap-through transition. No instability of the model was found in any of the computations carried out thereby suggesting that this phenomenon was indeed related to the near cancelation of terms and further demonstrating the benefit of the revised identification of Eqs (18)-(22).

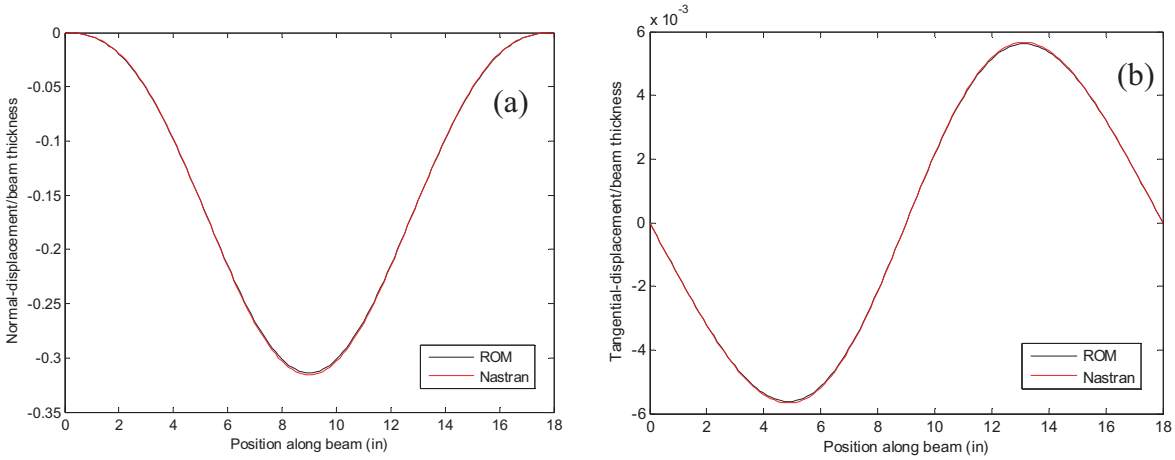

Figure 4. Comparison of static responses predicted by Nastran and by the reduced order model, curved beam, P = 1.7 lb/in. (a) Normal and (b) tangential displacements.

The assessment of the reduced model in matching the full finite element results was carried out in two phases corresponding to the two branches, left and right, of the response curve of Fig. 3. Shown in Fig. 4 are the normal and tangential displacements obtained at the load of

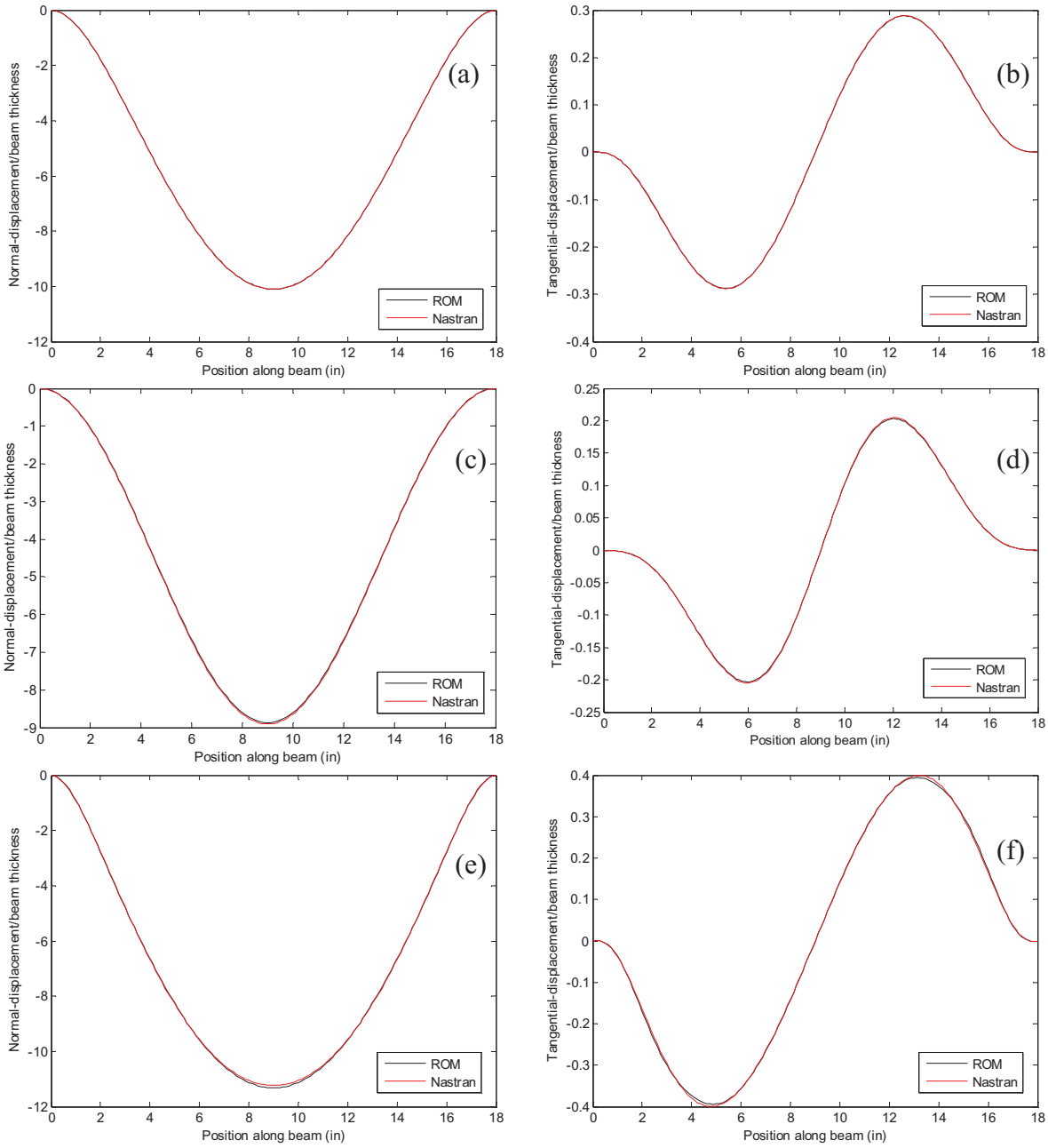

Figure 5. Comparison of static responses predicted by Nastran and by the reduced order model, curved beam, (a), (b) P = 3 lb/in, (c), (d) P = 1 lb/in (right branch), (e), (f) P = 10 lb/in. (a),(c),(e) Normal and (b),(d),(f) tangential displacements.

P = 1.7lb/in which are typical of the left branch. An excellent match between Nastran and reduced order model results is obtained. A similar analysis was conducted with loading conditions on the right branch and shown in Fig. 5(a) and 5(b) are the normal and tangential displacements obtained for P = 3 lb/in. Both Nastran and reduced order models were then unloaded to P = 1 lb/in, see Fig. 5(c) and 5(d). Finally, a load of P = 10 lb/in was also considered and the responses are shown in Fig. 5(e) and 5(f). In all of these cases, an excellent match is obtained between the full finite element model results and the reduced order model predictions. Additional comparisons, in particular with other good reduced order models, are presented in [17]. Clearly, the identification algorithm based on Eqs (18)-(22) has led to very reliable reduced order models.

6 CYLINDRICAL SHELL VALIDATION CASE

The second validation example considered is a thin-walled cylindrical shell of thickness h=0.28mm and radius 0.125m, as shown in Fig. 6. It has a main body of length 0.144m and a fret of length 0.019m. The fret (Young's modulus 200000MPa) is slightly stiffer than the main body (Young's modulus 180000MPa), and they have the same Poisson's ratio of 0.3.

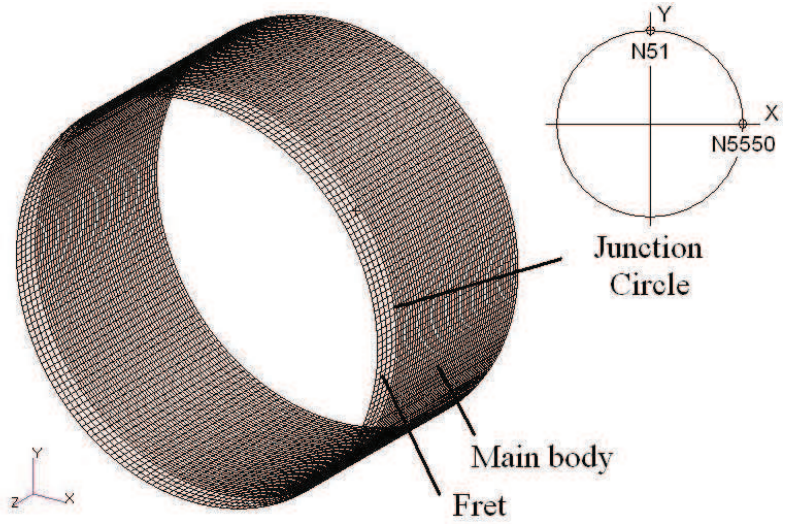

Figure 6. Finite element model of the shell.

The shell is clamped at the end of the main-body side and free to slide at the end of the fret side (free translational degrees of freedom and fixed rotational degrees of freedom). It is subjected to a longitudinal tension and a transverse force in the negative Y-direction along the junction circle of the main body and the fret. In the present study, the longitudinal tension is fixed at $F_z = 41\,N$, while the transverse force varies from $F_y = 0$ to $-50N$.

A finite element model of the shell was generated using MSC/Patran. This model has 10800 CQUAD4 elements and 11000 nodes. The nonlinear static responses of the shell to the aforementioned loads are computed using MSC/Nastran.

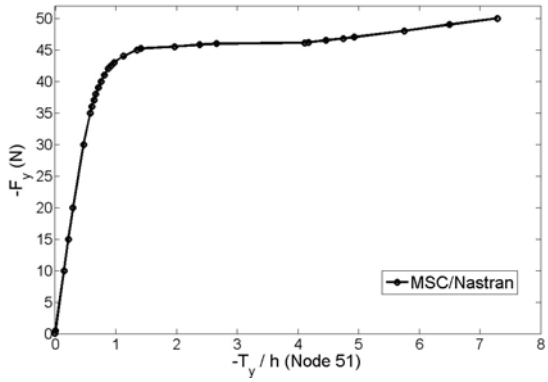

Figure 7. Displacement vs. load curve for the shell, node 51 Y displacement.

A typical force-displacement curve is shown in Fig. 7, in which the displacement in the Y-direction at node 51 against the negative F_y is plotted. The displacement is scaled by the

thickness of the shell. As shown in Fig. 6, node 51 is located on the *Y*-axis of the junction circle. Since the force is applied in the *Y*-direction across this plane, node 51 is a representative point for one to observe the response.

From Fig. 7, it can be seen that the response is linear up to $F_y = -30N$. The deformed shape of the shell at $F_y = -30N$ is shown in Fig. 8. In this figure and the following figures showing the deformed shapes, the deformation is magnified by 10 times to demonstrate the feature of the response clearly. One can see the response already shows a wrinkling behavior in the area in parallel to the *Y*-axis.

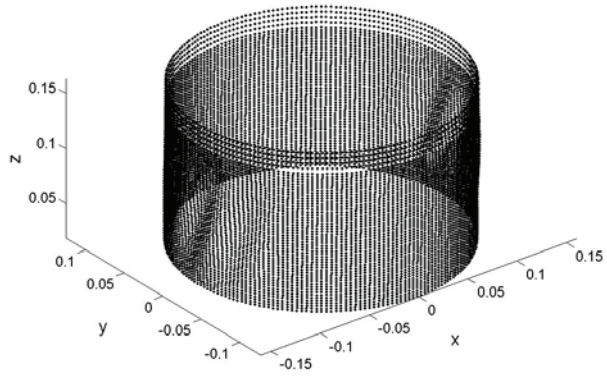

Figure 8. Deformation of the shell, $F_y = -30N$.

As F_y is increased, the wrinkling range of the response gradually extends and the magnitude becomes larger. This can be seen from the deformed shapes at $F_y = -40N$ and $-45N$ as shown in Fig. 9.

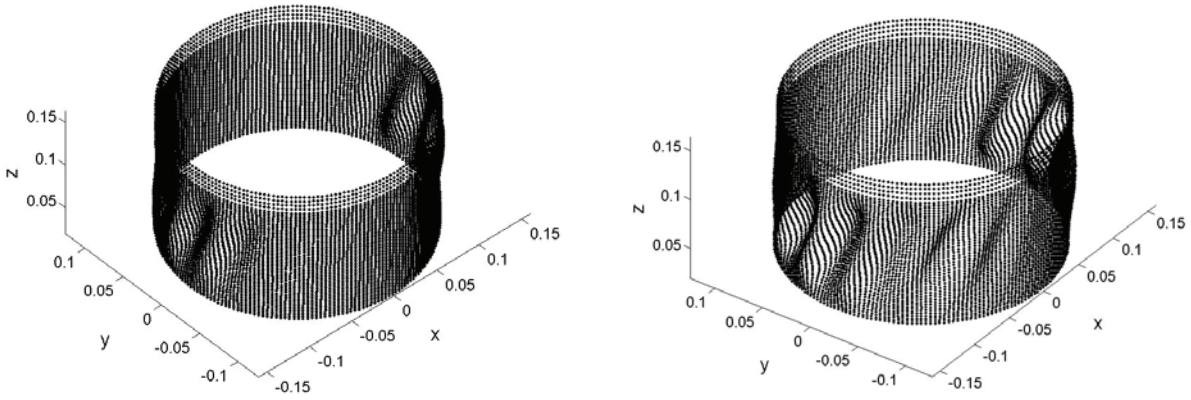

(a) (b)

Figure 9. Deformation of the shell, (a) $F_y = -40N$,(b) $F_y = -45N$.

When F_y is further increased from $-45N$ to $-47N$, the deformed shape undergoes a significant change. As seen from Fig. 10, which shows the deformed shape at $F_y = -47N$, the range of wrinkling is almost extended to the entire shell, and the magnitude is much larger than in previous figures. This can also be seen in the *Y*-displacement of node 51 as

shown in Fig. 7, which actually increases from $1.35h$ at $F_y = -45N$ to $4.93h$ at $F_y = -47N$.

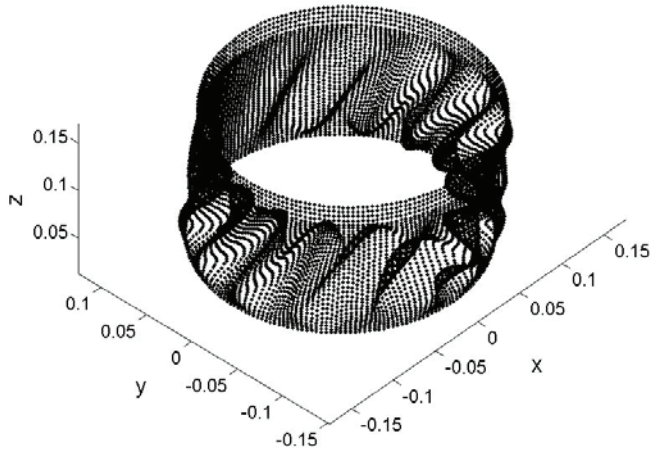

Figure 10. Deformation of the shell, $F_y = -47N$

Considering the complexity of the wrinkling behavior, this first investigation focuses solely on the development of a reduced order model that captures the shell behavior for forces F_y up to $-45N$.

The basis of linear modes used in the modeling of the curved beam may not be efficient for the shell model, Therefore, the technique of proper orthogonal decomposition (POD) is used to extract the basis functions for the reduced order modeling of the shell, e.g. see [18] for a review. The set of nonlinear static responses for F_y varying from $-0.05N$ to $-45N$ ($-F_y$ = 0.05, 0.5, 10, 20, 30, 35, 37, 38, 39, 40, 41, 42, 43, 44, 45*N*) are taken as the set of data for the POD analysis. Prior to the analysis, the responses are scaled such that the maximum component of each response is unity. In this way, the contributions of the responses to the basis of POD modes are equally weighted at the low and the high force levels. The POD analysis is implemented using the MATLAB function "svd" for singular value decomposition. From the analysis, the first 6 POD modes are found to be able to represent the responses well, thus are chosen as the basis functions of the reduced order model.

The next step is the identification of the nonlinear stiffness coefficients and this will be accomplished by relying on Eqs (18)-(22) with two baseline solutions, corresponding to the projection of the full finite element results for $F_y = -42N$ and $F_y = -45N$.

The developed reduced order model is validated against the MSC/Nastran results for a series of F_y values. Included in those are three "blind" F_y values, that is, $F_y = -15N$, $-36N$ and $-42.5N$, which were not used in the database for the POD analysis. In the validation, the displacements in the *Y*- and *Z*- directions of two nodes, node 51 and node 5550, are presented. The displacement in the *X*-direction is generally small and thus not discussed here. As shown in Fig. 7, nodes 51 and 5550 are located on the *Y*- and the *X*- axis of the junction circle, respectively.

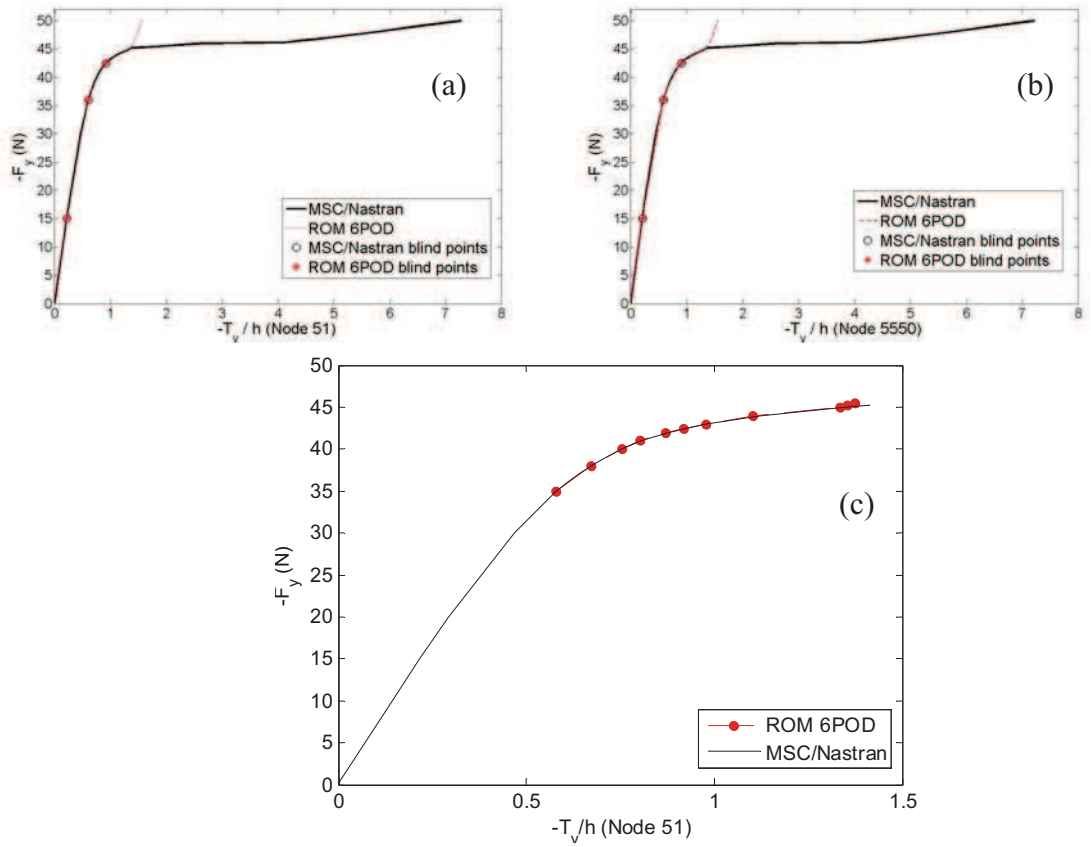

Figure 11. Displacement vs. load curve for the shell obtained with Nastran and with the reduced order model. (a) Node 51 *Y* displacement, (b) Node 5550 *Y* displacement, (c) Node 51 *Y* displacement, zoomed.

Shown in Fig. 11 are comparisons of the *Y*-displacements of the two nodes for the reduced order model (ROM 6POD) and the MSC/Nastran. The results at the three "blind" points are marked in particular. It can be seen that an excellent matching is obtained for F_y up to $-45N$. It should be noted that the comparison is also made for F_y beyond $-45N$, and the current model does not capture correctly the response. This is expected since the basis of the current model is derived from the data below $F_y = -45N$, and it does not represent the response beyond this value well. Yet, until that threshold the agreement between the Nastran and ROM predictions is excellent, see in particular Fig. 7(c).

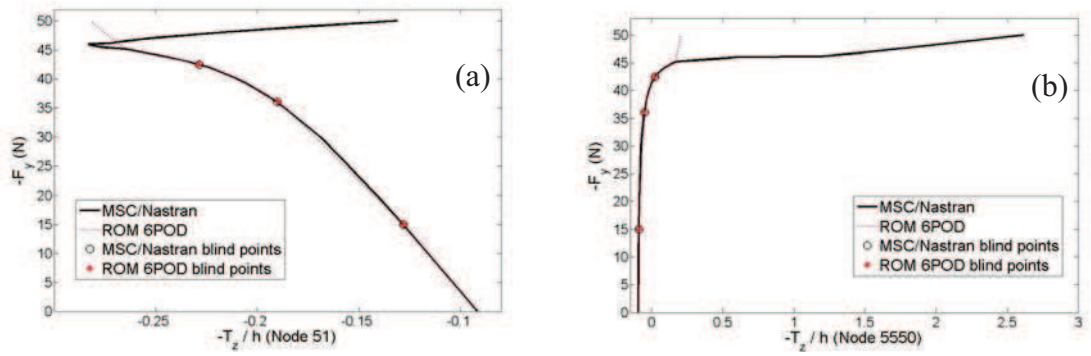

Figure 12. Displacement vs. load curve for the shell obtained with Nastran and with the reduced order model. (a) Node 51 *Z* displacement, (b) Node 5550 *Z* displacement,

A comparison of the *Z*-displacements of the two nodes predicted by the reduced order model and Nastran is shown in Fig. 12 and a similar matching of these results is observed.

A final assessment of the reduced order model is carried out in Figs 13 and 14 which show the deformed shapes predicted by both the reduced order model and Nastran at two "blind" force values, $F_y = -36N$ and $-42.5N$. The wrinkling behavior of the shell is very similar in both cases supporting further the accuracy of the reduced order model.

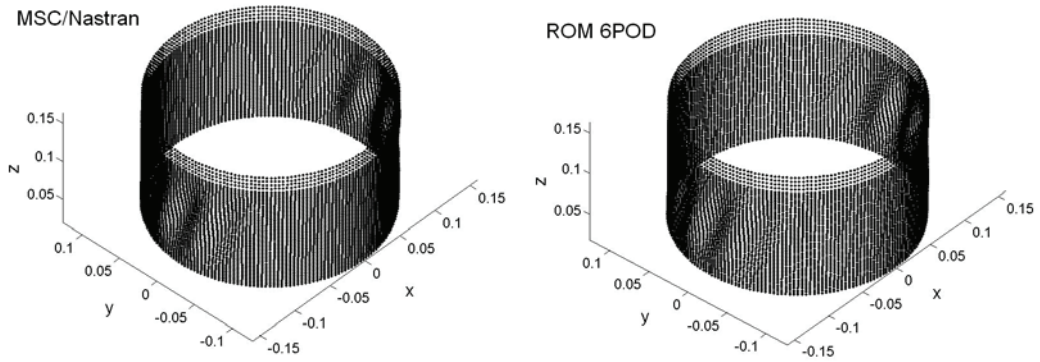

Figure 13. Deformation of the shell, $F_y = -36N$.

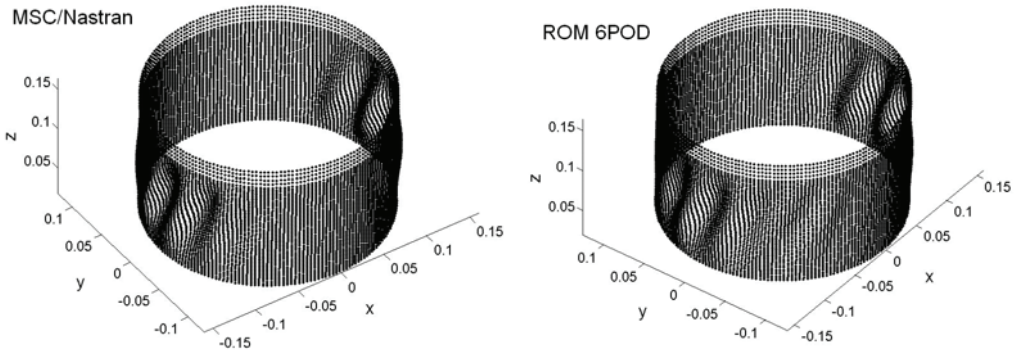

Figure 14. Deformation of the shell, $F_y = -42.5N$.

7 SUMMARY

The present investigation focused on a revisit and extension of existing approaches for the reduced order modeling of the geometrically nonlinear response of structures. Difficulties, i.e. instability of the reduced order model, encountered in the past in connection with a curved beam were first analyzed. This effort then served as the basis for the formulation of a revised identification procedure of the parameters of the reduced order model, see Eqs (18)-(22). The application of this procedure to the previous curved beam model removed the instability issue and led to an excellent matching of reduced order model and finite element predictions for a broad range of external loading. On this basis, a complex structural model of a shell subjected to bi-directional loading and exhibiting a wrinkling deformation was considered and its reduced order modeling was undertaken. An excellent match of the nonlinear finite element response was achieved with the reduced order model until the wrinkling extends to the entire structure. The present results extend previous validation

studies in demonstrating the worth of reduced order modeling of nonlinear geometric structures.

8 REFERENCES

[1] MCEWAN, M.I., WRIGHT, J.R., COOPER, J.E., LEUNG, A.Y.T., *A combined modal/finite element analysis technique for the dynamic response of a nonlinear beam to harmonic excitation*, Journal of Sound and Vibration, 2001, 243, pp. 601-624.
[2] HOLLKAMP, J.J., GORDON, R.W., SPOTTSWOOD, S.M., *Nonlinear modal models for sonic fatigue response prediction: a comparison of methods*, Journal of Sound and Vibration, 2005, 284, pp. 1145-1163.
[3] RADU, A., YANG, B., KIM, K., MIGNOLET, M.P., *Prediction of the dynamic response and fatigue life of panels subjected to thermo-acoustic loading*, 45th Structures, Structural Dynamics, and Materials Conference, Palm Springs, Apr. 2004, Paper AIAA-2004-1557.
[4] PRZEKOP A., RIZZI S.A., *Nonlinear reduced order random response analysis of structures with shallow curvature*, AIAA Journal, 2006, 44, pp. 1767-1778.
[5] GORDON R.W., HOLLKAMP, J.J., *Reduced-order modeling of the random response of curved beams using implicit condensation*, 47th Structures, Structural Dynamics, and Materials Conference, Apr. 2006, Paper AIAA-2006-1926.
[6] SPOTTSWOOD, S.M., HOLLKAMP, J.J., EASON, T.G., *On the use of reduced-order models for a shallow curved beam under combined loading*, 49th Structures, Structural Dynamics, and Materials Conference, Schaumburg, Apr. 2008, Paper AIAA-2008-1873.
[7] KIM, K., KHANNA, V., WANG, X.Q., MIGNOLET, M.P., *Nonlinear reduced order modeling of flat cantilevered structures*, 50th Structures, Structural Dynamics, and Materials Conference, Palm Springs, May 2009, Paper AIAA-2009-2492.
[8] KIM, K., WANG, X.Q., MIGNOLET, M.P., *Nonlinear reduced order modeling of functionally graded plates*, 49th Structures, Structural Dynamics, and Materials Conference, Schaumburg, Apr. 2008, Paper AIAA-2008-1873.
[9] PEREZ, R., WANG, X.Q., MIGNOLET, M.P., *Nonlinear reduced order models for thermoelastodynamic response of isotropic and FGM panels*, 2011, AIAA Journal, 49, pp. 630-641.
[10] PEREZ, R., WANG, X.Q., MIGNOLET, M.P., *Reduced order modeling for the nonlinear geometric response of cracked panels*, 52nd Structures, Structural Dynamics and Materials Conference, Apr. 2011, Denver, Paper AIAA 2011-2018.
[11] SPOTTSWOOD, S.M., EASON, T.G., WANG, X.Q., MIGNOLET, M.P., *Nonlinear reduced order modeling of curved beams: a comparison of methods*, 50th Structures, Structural Dynamics, and Materials Conference, Palm Springs, May 2009. Paper AIAA-2009-2433.
[12] RIZZI, S.A. PRZEKOP, A., *System identification-guided basis selection for reduced-order nonlinear response analysis*, 2008, Journal of Sound and Vibration, 315, pp. 467-485.
[13] PRZEKOP, A. RIZZI, S.A., *Nonlinear reduced-order analysis with time-varying spatial loading distributions*, 2009, Journal of Aircraft, 46, pp. 1395-1402.
[14] MURAVYOV, A.A., RIZZI, S.A., *Determination of nonlinear stiffness with application to random vibration of geometrically nonlinear structures*, 2003, Computers and Structures, 81, pp. 1513-1523.
[15] FUNG, Y.C., TONG, P., *Classical and Computational Solid Mechanics*, 2001, World Scientific, River Edge, New Jersey.
[16] BONET, J., WOOD, R.D., *Nonlinear Continuum Mechanics for Finite Element Analysis*, 1997, Cambridge University Press, Cambridge.

[17] CHANG, Y.W., *Reduced Order Modeling for the Nonlinear Geometric Response of a Curved Beam*, 2011, M.S. Thesis, Arizona State University.
[18] KERSCHEN, G., GOLINVAL, J.-C., VAKAKIS, A.F., BERGMAN, L.A., *The method of proper orthogonal decomposition for dynamical characterization and order reduction of mechanical systems: an overview*, 2005, Nonlinear Dynamics, 41, pp. 147-169.